Effects of molecular rotation on densities in doped 4He clusters

M. V. Patel, A. Viel, F. Paesani, P. Huang, and K. B. Whaley

View Online   Export Citation

ARTICLES YOU MAY BE INTERESTED IN

Effects of molecular rotation on densities in doped ^{4}He clusters

M. V. Patel[a)]
Departments of Physics and Chemistry and Kenneth S. Pitzer Center for Theoretical Chemistry, University of California, Berkeley, California 94720-1460

A. Viel,[b)] F. Paesani, P. Huang, and K. B. Whaley[c)]
Department of Chemistry and Kenneth S. Pitzer Center for Theoretical Chemistry, University of California, Berkeley, California 94720-1460

The effects of including rotational degrees of freedom on helium solvation densities in molecule-doped helium clusters are investigated for a variety of molecules. Helium densities and cluster energetics are calculated with diffusion Monte Carlo methods. The rotationally induced changes in the helium density distributions are examined and quantified with a theoretical estimator applicable to molecules of arbitrary symmetry. This analysis leads to a discussion of adiabatic following of molecular rotation in a solvating helium environment. We make a detailed comparative study of the effect of molecular rotation as a function of four impurity molecules with varying mass and symmetry: SF$_6$, OCS, HCN, and benzene (C$_6$H$_6$). We find that even for the heaviest rotors, only a fraction of the solvating helium density adiabatically follows the molecular motion in the quantum ground state. For the lightest molecule, HCN, a negligible degree of adiabatic following is found. A discussion of the various definitions is presented to clarify the meaning of adiabatic following, and its applicability to dynamical models of quantum rotation in helium droplets is evaluated in light of the quantitative findings of incomplete adiabatic following established here. © *2003 American Institute of Physics.* [DOI: 10.1063/1.1545106]

I. INTRODUCTION

Interpretation of the phenomenon of apparent free rotation of small molecules and complexes in ^{4}He droplets has generated considerable theoretical activity in recent times.[1–9] This phenomenon is now widely observed in a broad range of infrared and microwave experiments,[10,11] where it is seen to be a characteristic of the superfluid solvation environment provided by the bosonic isotope, ^{4}He at temperatures $T \sim 0.4$ K. No spectroscopic signature of rotational states is seen in the fermionic ^{3}He droplets,[12] a feature that is understood in terms of the high density of single-particle excitations in the fermionic quantum liquid, causing efficient scattering and decay of rotational excitations as in classical liquids.[2]

Several approaches have been advanced to model the rotational dynamics of molecules that are solvated by the unique quantum fluid environment provided in ^{4}He. These include direct calculation of cluster energy levels correlated with molecular excited rotational levels,[1,3,8,9] a microscopic two-fluid theory of helium response to molecular rotation based on path integral decompositions of the solvating helium density into local superfluid and molecular-interaction induced nonsuperfluid components,[4,7] and hydrodynamic models for helium response to classical molecular rotation.[5–7,13,14] Of these, the direct calculations currently

provide the most complete theoretical description, with full incorporation of the molecular rotational degrees of freedom in microscopic quantum calculations of rotational excitations of the doped clusters. These calculations employ diffusion Monte Carlo (DMC) methods, and may provide either energy levels alone, or energy levels with associated multidimensional cluster wave functions. To date, direct calculations have been made using either fixed node diffusion Monte Carlo[3] or the projection operator imaginary time spectral evolution methodology.[1,8,9] The latter is more powerful, allowing the limitations of fixed node constraints to be overcome and exact excited states to be obtained, as demonstrated in Refs. 8 and 9.

The first DMC studies incorporating molecular rotation gave rise to the notion of *adiabatic following* of the molecular rotation by some fraction of the helium density.[3] This notion, which will be discussed in detail in the latter part of this paper, plays a key role in the other two theoretical approaches, i.e., in the microscopic two-fluid theory and in the hydrodynamic model. The formulations of the microscopic two-fluid theory and hydrodynamic models made to date rely on theoretical estimates of the helium response to molecular rotation that are based on assumptions of either complete or partial adiabatic following of the molecular rotational motion by the solvating helium density. However, the solvating helium densities that have been used in calculations with these approaches to date have all been calculated for nonrotating molecules, within the implicit assumption that the density will be similar for a rotating molecule. The DMC approaches offer a direct method to assess the validity of this assumption, which is often loosely referred to as the assumption of

[a)]Current address: Lawrence Livermore National Laboratory, L-405, Livermore, CA 94550.
[b)]Current address: Technische Universität München, D-85747 Garching bei München, Germany.
[c)]Electronic mail: whaley@socrates.berkeley.edu

adiabatic following of the molecular rotation by the helium density. A primary theme of this paper is to examine in detail the extent of validity of this assumption, and to show with demonstrations for a number of molecules of different mass and symmetry that this assumption is not correct and that the helium density distribution is indeed quite sensitive to the presence or absence of molecular rotation.

A second theme of this paper is to show that making use of the intrinsic anisotropy of the molecule–helium interaction offers a route to quantification of the *extent* of adiabatic following, via an estimator that measures the effect of molecular rotation on the solvating helium density. We apply this estimator to the same set of molecules differing in both mass and shape, and show that it allows a systematic analysis of the extent of adiabatic following for a range of molecules relevant to experimental studies in helium droplets. In particular, we examine the extent of adiabatic following of the molecular rotation by helium for several small molecules of differing mass and molecular geometry. We analyze the behavior of SF_6, OCS, HCN, and benzene (C_6H_6). The first two provide a pair of relatively heavy molecules that differ in molecular symmetry, SF_6 being octahedral and OCS linear. OCS and HCN allow a comparison of the effect of molecular mass to be made, between two molecules possessing the same linear symmetry. Benzene represents an extreme case in the heavy regime, for which the molecule–helium interaction potential is much more anisotropic than the other examples.

The structure of the remainder of this paper is as follows: Section II gives a brief overview of the computational methods used in the calculations presented here, noting the various different estimators employed in calculation of the helium density and/or wave function. Section III presents results (comparison of densities obtained with and without the inclusion of molecular rotation) for the smallest molecule–helium complexes, $N=1$, containing a single helium atom, together with essential numerical details for each of the four molecules studied here. In Sec. IV we analyze and quantify the effect of rotations on these density distributions, with an estimator that compares the anisotropy of the density distribution in the cluster ground state when this is evaluated with and without molecular rotation. This estimator is then applied first to the $N=1$ clusters. Section V presents the corresponding analysis for larger cluster sizes ($N \leqslant 20$, containing up to one solvation shell), together with a discussion of the more complex set of factors that affect the helium density distributions and the estimator at these sizes. For the linear molecules OCS and HCN complexed with a single helium atom where it is possible to make exact calculations of excited state energies and wave functions, we also evaluate the difference in solvating helium density distributions between the $J=0$ and $J=1$ cluster rotational levels.

We summarize and provide a comparative discussion and conclusions for the interpretations of the rotational dynamics in helium droplets in Sec. VI.

II. THEORETICAL METHODS

The primary methodology employed here is the importance-sampled rigid body diffusion Monte Carlo algorithm (IS-RBDMC) that is developed and described in detail in Ref. 15. In general, all degrees of freedom (both rotational and translational) are importance-sampled in this approach. As a result, it can be used for calculation of both ground and excited state energies for molecules in helium clusters with full incorporation of the molecular rotational kinetic energy. This has allowed calculation of rotational states to be made within fixed node approximation,[3] as well as application of the more powerful projection operator spectral evolution methodology to the direct calculation of rotational excitations without nodal approximations.[8,9] Importance sampling of the molecular rotational degrees of freedom is important when these are strongly coupled with the translational and/or vibrational degrees of freedom of the cluster. This is the situation with heavier molecules, such as SF_6, OCS, and benzene. For weakly coupled molecules, such as the lighter HCN molecule, the importance sampling of rotations is less critical and may often be neglected.

We employ this full importance-sampled rigid body algorithm here for the ground states of the molecule-doped helium clusters, making use of explicit importance sampling of the molecular angular degrees of freedom as required. Trial wave functions and additional computational details are provided in the Appendix. Calculations are made for each molecule in ^4He_N, with and without the rotational kinetic energy of the molecule. Each of these pairs of calculations allows an assessment of the effect of quantum rotational motion of the molecule on the helium distributions in the molecular frame to be made. We find differences in both the energy and the helium density distributions between these pairs of calculations.

The difference in energy observed between the two cases derives from the fact that the rotation of the molecule inside the cluster is not a free motion but is hindered by the presence of helium atoms. This gives rise to a matrix zero point energy contribution that can be viewed as the effect of the hindered rotation and having a mixed rotational and vibrational character (i.e., libration). As a consequence the calculation without the kinetic term corresponding to the molecular rotation misses some part of the zero point energy of internal degrees of freedom of the full cluster. In the remainder of this paper, we refer to this difference as the "hindered rotation energy" increment.

Several approaches are used here to analyze the ground state helium densities in the molecular frame. While DMC yields exact ground state energies when numerically converged, expectation values of position operators may be subject to trial function bias when importance sampling algorithms are employed. This may be dealt with at several levels. It may be completely avoided by the use of descendant weighting,[16] requiring a significant increase in computational effort. It may be reduced by the use of extrapolation estimates such as the second-order estimator.[17] For very small clusters, e.g., the $N=1$ complexes we study here, the densities can be obtained from nonimportance sampled "unbiased" DMC, for which trial function bias is absent. For larger size clusters we may also use unbiased DMC, and simply examine the projections of the N-helium wave function into the molecular frame, rather than the density.[7] Addi-

J. Chem. Phys., Vol. 118, No. 11, 15 March 2003

Doped ^{4}He clusters   5013

tionally, since we are interested in comparisons between densities evaluated with and without rotation, if only radial trial functions are consistently used in both calculations and the cluster is less than a single solvation shell so that there is no extended radial structure, then there should be negligible bias on the helium angular distributions and hence on the adiabatic quantifier proposed here. Either mixed or second-order densities can be used in this situation. However, when the trial functions are anisotropic, care must be taken to assess the extent of trial function bias on the density differences found between the nonrotating and rotating molecule calculations. When the trial functions are highly optimized, it is expected that use of the second-order extrapolation should effectively reduce trial function bias on the difference between the densities from the two calculations.

In the calculations presented here, we have obtained consistent results using descendant weighting (benzene, OCS), second-order density estimators (OCS), mixed density estimators (SF_6, HCN), and unbiased DMC (SF_6, HCN, OCS). In addition, for SF_6 we have also made the corresponding analysis comparing wave function projections instead of densities, and find consistent results for the corresponding measures of adiabatic following (Sec. IV).

For the smallest cluster size, $N=1$, we use the collocation method[18–20] modified by Drucker and Higgins[21] in order to determine exact rotationally excited energy and wave functions for HCN and OCS as a function of total angular momentum J. This method is based on using basis set methods for the representation of the kinetic energy operator and grid points for the representation of the potential. The six-dimensional wave function is expanded onto basis set functions made of product of radial wave functions and Wigner matrices representing the relative rotation of the rigid body with respect to the atom, and the overall rotation. For both HCN and OCS, the ground state wave function obtained from collocation calculations is identical to the corresponding ground state function obtained from unbiased DMC. This is also the case when a nonrotating rigid body is used. For He–SF_6, we obtain excited state energies from unbiased DMC using the fixed-node approximation. In this scheme, a trial excited state nodal surface is imposed by rejecting walker moves which attempt to cross this surface, thus yielding an energy which is a variational upper bound to the lowest state of the same symmetry. For He–SF_6, we compute an approximate $J \approx j = 1$ excited state, where j is the spherical top angular momentum quantum number. This assumes that the total cluster angular momentum J can be approximately separated into the molecule angular momentum j and the helium angular momentum. For SF_6 in large helium clusters this approximation has been shown to give good agreement with experimentally observed rotational energy level spacings.[3] Note that this approximate angular momentum decoupling does not preclude a renormalization of the effective molecular moment of inertia, as discussed in Ref. 7.

III. ENERGIES AND HELIUM DENSITIES FOR $N=1$

A. SF_6

SF_6 lies in the dynamical regime of slow, heavy molecules in helium droplets,[7] possessing a gas phase rotational
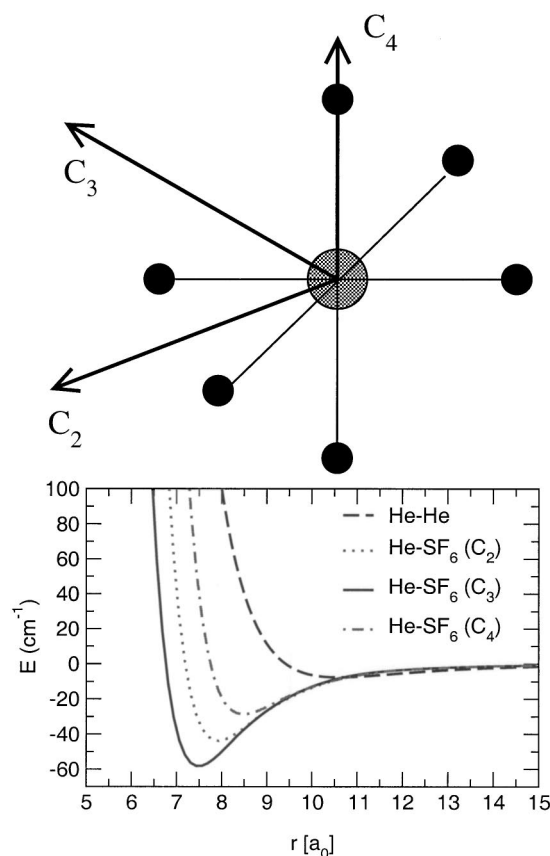

FIG. 1. (a) Schematic of the SF_6 molecule showing the high symmetry axes (C_2, C_3, and C_4). (b) Radial cuts of the SF_6–He potential (Ref. 23) along the high symmetry axes marked in (a). The He–He potential (Ref. 24) is also plotted for comparison.

constant $B_0 = 0.09$ cm^{-1} and mass 146 amu. The rotational constant decreases to 36% of B_0 in ^{4}He clusters.[22] The octahedral SF_6 molecule is shown together with its high symmetry axes (C_2, C_3, and C_4) in Fig. 1(a). The C_4 axes lie along the S–F bonds, the C_3 axes are located in the centers of the octahedral pockets (everywhere equidistant from the three delimiting C_4 axes), and the C_2 axes point toward the midpoint of a line segment connecting adjacent F atoms. The anisotropic SF_6–He interaction is modeled using the potential of Pack et al.[23] Cuts of this potential along the high symmetry axes are shown in Fig. 1(b). The He–He interaction[24] is also shown here, for ease of reference. The SF_6–He interaction potential has eight equivalent minima situated on the C_3 symmetry axes at a distance of 7.5 a_0 from the sulfur atom, each of which has a well depth of 58.285 cm^{-1}. For the purposes of studying how the helium density is distributed around the molecule, we find it useful to define two special axes along which the density is examined. One of these is an axis favorable for helium density, and the other is an axis unfavorable for helium density (see Sec. IV B). For SF_6, the obvious choice for the "favorable" (includes region of lowest potential energy) axis, F, is the C_3 axis. The potential possesses two saddle points with respect to rotation around the molecule. They lie on the two other symmetry axes, C_4 and C_2, which are thus two possible candidates for the special "unfavorable" U axis.

TABLE I. Unbiased and biased (importance sampled) DMC energies for the SF_6–He complex. The numbers in parentheses give one standard deviation statistical errors in the last digits. The energies are in agreement with the value of -25.81 cm^{-1} obtained by finite basis set/discrete variable representation (FBR/DVR) calculations. This FBR/DVR value is converged, i.e., it is stable when the unsymmetrized basis set size is increased from 19 890 to 33 930.

	DMC (cm^{-1})	DMC (no rotations) (cm^{-1})
Unbiased	$-26.0(1)$	$-26.7(2)$
Biased	$-25.8(2)$	$-26.7(2)$

We analyze the effect of rotations on the helium density surrounding the dopant SF_6 here with both importance-sampled and unbiased (pure) DMC. The importance sampling is made with the IS-RBDMC scheme described in Ref. 15, using the isotropic trial wave function described in the Appendix. For SF_6, a spherical top molecule, calculations are carried out in the fixed laboratory frame implementation.[15] In the importance sampled analysis we look at mixed densities, and in the unbiased DMC case, we examine the single particle wave function. In both instances, these quantities are projected into the molecular frame. The ground state energies obtained for both the importance-sampled and unbiased calculations are listed in Table I. The ground state energies obtained with rotations included are in good agreement with an independent discrete variable representation (DVR) calculation.[15] The energy increment due to the hindered rotations is about 0.70 cm^{-1}. Note that this is considerably greater than the spacing between the lowest free-rotor energy levels ($2B_0 = 0.18$ cm^{-1}). As discussed previously, this reflects the fact that the hindered rotation has some vibrational character and implies that adding the molecular rotational degrees of freedom to a molecule–helium cluster containing a nonrotating molecule will have a more dramatic effect on the system than a low lying rotational excitation of the molecule would do. This will be confirmed in Sec. IV D where we specifically examine the effect of increasing the molecular rotational state.

The ground state helium densities along the symmetry axes of the SF_6 molecule, calculated with and without rotation, are compared in Fig. 2. In all cases, we average over equivalent symmetry axes in sampling the helium densities.
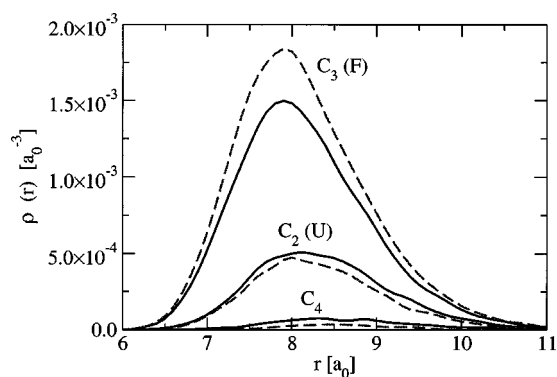

FIG. 2. Comparison of radial helium density profiles obtained with SF_6 rotation (solid lines) and without SF_6 rotation (dashed lines) along the three symmetry axes for SF_6–He (see Fig. 1).
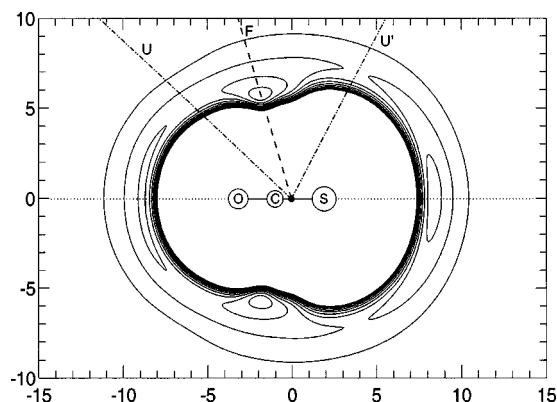

FIG. 3. Contour lines of the potential energy surface for the OCS–He interaction (Ref. 26), showing also the locations of the oxygen, carbon, and sulfur atoms. The lowest contour line is at -40 cm^{-1}, and the line increment is 10 cm^{-1} (the outermost contour displayed is thus at -10 cm^{-1}). The filled circle indicates the position of the OCS center-of-mass. F, U, and U' denote privileged directions passing through this point (see the text). Distances are shown in atomic units (a_0).

The effect of the rotations is to reduce the localization around the potential minimum (reduction of density along C_3 axis), and to increase the density along the less favorable directions (along C_2 and C_4 axes). Consequently there is some overall smearing out of the density in the molecular frame as a result of including the molecular rotational motion.

These differences in both energies and density profiles imply that even in the ground state, molecular rotations do have a noticeable effect on the properties of the cluster. The fact that the densities obtained including rotations do nevertheless closely resemble those obtained with a nonrotating molecule implies that the helium density is able to *adiabatically follow* the molecular rotation to an appreciable extent. A full discussion of this concept and a more quantitative description of this observation will be provided in Sec. IV C 1.

B. OCS

The OCS molecule is a slow linear rotor lying in the same dynamical regime as SF_6, although it is somewhat lighter. Its rotational constant in the gas phase is $B_0 = 0.207$ cm^{-1} and its mass is 60 amu. In ^{4}He droplets it undergoes a decrease of rotational constant similar to that of SF_6, with a reduction to $B = 0.07$ cm^{-1}, i.e., to 34% of its gas phase value.[25] In the present work we have used a full potential energy surface based on the *ab initio* He–OCS interaction previously calculated by one of us (F.P.), using density functional theory together with dispersion contributions.[26] This He–OCS potential energy surface, defined in Jacobi coordinates (r, θ), is shown in Fig. 3. The global minimum of -46.02 cm^{-1} is located at $r = 5.98$ a_0 and $\theta = 108.0°$. There are other two secondary minima for the two collinear geometries. The first, at $\theta = 0°$ (sulfur side), has a well depth of -34.56 cm^{-1} and is located at 8.36 a_0. The second local minimum, at $\theta = 180°$ (oxygen side), has a comparable well depth of -32.01 cm^{-1} and is located at 8.93 a_0 from the OCS center-of-mass. The two saddle points are located, respectively, at $\theta = 61.7°$ and $\theta = 132.1°$. In
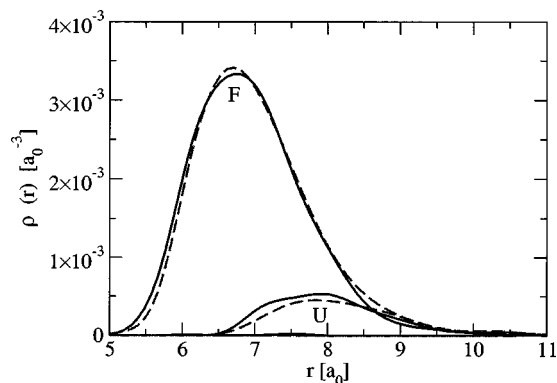
FIG. 4. Comparison of radial helium density profiles obtained with OCS rotation (solid lines) and without OCS rotation (dashed lines) along the privileged axes F and U for OCS–He (see Fig. 3).

Fig. 3 we have also indicated three privileged directions starting from the OCS center-of-mass and passing, respectively, through the global minimum point (F), the first saddle point (U′), and the second saddle point (U). The binding energy of a single helium atom in this potential is -15.84 cm^{-1}.[26] The ground state energy calculated with a nonrotating OCS molecule is -17.06 cm^{-1}, resulting in a hindered rotation energy increment of 1.2 cm^{-1}.

Figure 4 shows the ^{4}He densities along the F and U axes, derived from calculations with molecular rotation (solid lines) and without molecular rotation (dashed lines). These densities are derived as second-order extrapolations from IS-RBDMC calculations in the mixed frame implementation,[15] using the anisotropic trial wave function described in the Appendix. The density along the U′ axis is negligible at all distances and is therefore not shown. We see that the densities obtained with molecular rotation appear qualitatively similar to those obtained with a nonrotating molecule, but that there is a noticeable angular smearing out of the helium density for the rotating molecule. This situation is very similar to that seen earlier for SF$_6$, and suggests that the helium density is similarly able to *adiabatically follow* the OCS rotational motion to a significant but incomplete extent.

C. Benzene (C$_6$H$_6$)

Benzene is an oblate symmetric rotor with gas phase rotational constants $A_0 = 0.188$ cm^{-1}, $C_0 = 0.0938$ cm^{-1}, and a mass of 78.11 amu. This puts it in the same mass and moment of inertia regime as SF$_6$ and OCS. No rotational spectrum of benzene has been measured in ^{4}He droplets to date, although rotational constants have been measured for the $N=1$ complex.[27] In comparison to both SF$_6$ and OCS, the helium–benzene interaction is markedly more anisotropic. We use here an analytical fit[14] to *ab initio* data of Hobza *et al.*[28] There are two equivalent global minima of $V_0 = -66.01$ cm^{-1}, located on the molecule C_6 symmetry axis at a distance of $z = \pm 6.18$ a_0 from the benzene plane. There are also twelve equivalent secondary minima of $V_0' = -43.47$ cm^{-1}. These secondary minima correspond to a helium atom situated roughly between two neighboring hydrogen atoms, six above and six below the benzene plane. The global minimum on one side of the molecule is con-
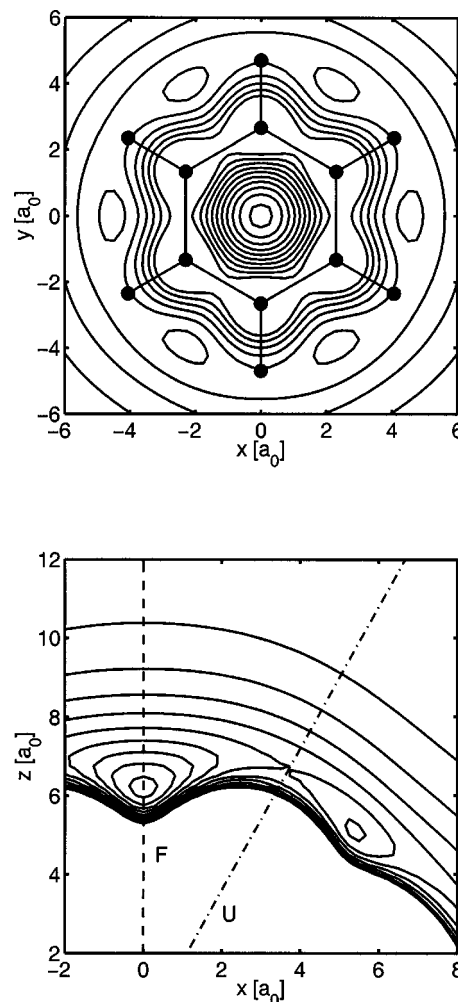

FIG. 5. Upper panel: cut of the benzene–He potential through the global minima along a plane parallel to the benzene molecule, at a distance of $z = 6.18$ a_0 above the benzene plane. The orientation of the molecule is shown by marking the carbon and hydrogen positions on the $z=0$ plane by filled circles. Lower panel: cut of the benzene–He potential along the $y = 0$ plane, intersecting a global minimum at (0,6.18), a saddle point at (3.72,6.69), and a secondary minimum at (5.37,5.10). The axes F and U pass through the global minimum and saddle point, respectively. The contour lines on both contour plots run from -63 cm^{-1} to zero in increments of 7 cm^{-1}.

nected to each of the six secondary minima on the same side via a saddle point of $V_b = -35.29$ cm^{-1}. These saddle points, twelve in all, are located roughly above and below the C–C bonds. A cut of the potential through the global minimum along a plane parallel to the benzene plane is shown in the upper panel of Fig. 5. The corresponding lower panel shows a cut through a plane perpendicular to the molecule that intersects a global minimum, a secondary minimum, and one saddle point on the potential surface. The binding energy of a single helium atom in this potential is $-18.65(3)$ cm^{-1},[29] increasing to $-21.61(2)$ cm^{-1} if the molecule is nonrotating. This results in a relatively large hindered rotation energy increment of 2.97 cm^{-1}. Comparison of this value with the corresponding values for SF$_6$ and OCS above implies that the magnitude of the hindered rotation energy increment (and its value relative to the free rotation B_0) is correlated in a general sense with the extent of anisot-
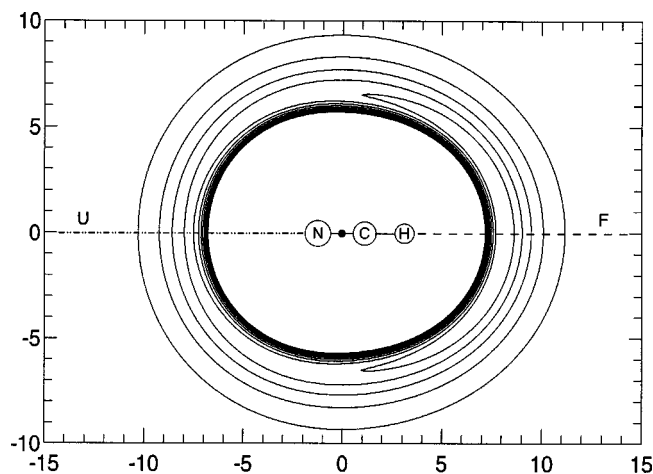
FIG. 6. Contour lines of the potential energy surface for the HCN–He interaction, showing also the locations of the hydrogen, carbon, and nitrogen atoms. The lowest contour line is at -25 cm^{-1} and the increment is 5 cm^{-1} (the outermost contour displayed is thus at -5 cm^{-1}). The filled circle indicates the position of the HCN center-of-mass. The F axis ($\theta=0$) is shown as the dashed half line, the U axis ($\theta=\pi$) as the dot-dashed half line. Distances are shown in atomic units (a_0).
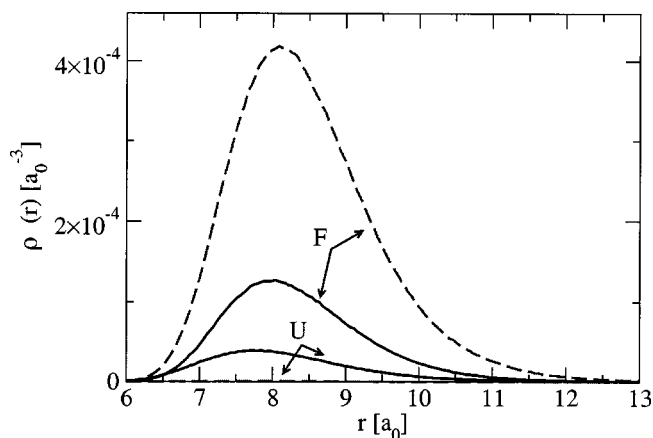

FIG. 7. Comparison of radial helium density profiles obtained with HCN rotation (solid lines) and without HCN rotation (dashed lines) along the privileged axes F ($\theta=0$) and U ($\theta=\pi$) for HCN–He.

ropy of the helium–molecule interaction, consistent with a significant contribution from relative vibrational motion.

Calculations for benzene–He$_N$ clusters were carried out with the IS-RBDMC algorithm in the mixed frame representation,[15] using the trial functions described in the Appendix, and evaluating the helium densities with descendant weighting.[16,29] For $N=1$, the helium density is strongly confined along the molecular C_6 axis, with a single peak located over the global potential minimum, as expected from the topology of the interaction potential. The position of this density maximum is in good agreement with experimental estimates for $N=1$.[14,27,29] The most obvious choice for the F direction is along the C_6 axis. We define the U direction to be an axis originating at the benzene center-of-mass, and passing through a saddle point V_b. There are thus two equivalent F axes, and twelve equivalent U axes.

D. HCN

The HCN molecule is a much faster rotor than the three previous molecules. Its rotational constant in the gas phase is $B_0=1.47$ cm^{-1}. This value is reduced by only 17% in helium clusters, to 1.20 cm^{-1}.[30,31] This molecule is also a much lighter molecule, with a mass of 27 amu (compared to 146 amu for SF$_6$, 60 amu for OCS, and 78 amu for C$_6$H$_6$).

For the HCN–He interaction we use the potential 1E8 derived by Atkins and Hutson.[32] This potential, based on both *ab initio* calculations and on spectroscopic data, is expressed as a function of the Jacobi coordinates (r,θ) of the helium atom with respect to the linear HCN molecule. We define a reference frame having the z axis lying along the HCN molecule with hydrogen on the positive side, and having x and y axes perpendicular to this, in two arbitrary but mutually perpendicular directions. The geometry of the potential minimum is linear ($\theta=0$), with the helium atom situated close to the hydrogen atom at a distance of $r=7.94$ a_0 from the center-of-mass of HCN, as depicted in Fig. 6, and

an energy of -29.6 cm^{-1} at the potential minimum. The saddle point of the interaction potential corresponds also to a linear configuration but with the helium atom now on the nitrogen side ($\theta=\pi$). These two geometries allow us to define two privileged axes for analyzing the density modulations. The favorable axis, F, is thus the positive z axis, with $\theta=0$, and the unfavorable axis, U, is the negative z axis, with $\theta=\pi$. These axes are shown, respectively, as dashed and dot-dashed horizontal lines in Fig. 6. This potential gives a ground state energy of -9.66 cm^{-1} for the HCN–He complex. The corresponding ground state energy with a nonrotating HCN molecule is -11.20 cm^{-1}, resulting in a hindered rotation energy increment of 1.55 cm^{-1} for HCN.

The effect of molecular rotation is studied using IS-RBDMC, employing the trial functions described in the Appendix and the mixed frame implementation.[15] The helium densities are evaluated here as mixed densities. As was done for SF$_6$ earlier, we have confirmed that the use of unbiased DMC leads to the same conclusions as derived from mixed densities.

Figure 7 shows the helium density profiles along the two axes F and U from HCN. For this light molecule we see that elimination of the molecular rotation has a very strong effect on the helium density. The calculations without rotation now show considerably more structure compared to the calculations with rotations. Thus the density profiles calculated with molecular rotation included are more smeared out, similar to the situation for SF$_6$ and OCS described earlier. However, for the lighter HCN molecule the difference is now far more dramatic. Additional demonstrations of this difference for HCN are provided in Fig. 3 of Ref. 15 and in Ref. 8. When rotations are not included, the helium density is quite localized, and its value at $\theta=\pi$ (U) is nearly zero.

IV. ANALYSIS OF EFFECTS OF ROTATION

A. The notion of adiabatic following

For a molecule that is deep inside a cluster, a spherically averaged, isotropic molecule–helium potential would give rise to an isotropic solvating helium density. When the inter-

action has angular dependence, however, the concept of *adiabatic following* often comes into play. Loosely speaking, the idea is that the rotating molecule drags some of the surrounding helium density with it. Adiabatic following can be discussed in either a classical or quantum mechanical dynamical framework. In a classical context, adiabatic following is said to hold when the helium density around a rotating molecule is independent of the speed of molecular rotation (up to some critical angular velocity determined from the time scale of the fluid's response). An energetic criterion for existence of such classical adiabatic following of the solvating helium density was given in Ref. 7, by comparing the magnitude of kinetic energy for classical rotation of the first shell helium solvation density around a given axis in the molecular frame with the corresponding potential energy derived from the molecule–helium interaction potential. In a quantum context, adiabatic following holds when the helium density in the rotating molecular frame is independent of the molecular rotational state. Determining the validity of adiabatic following in this context requires a comparative study of the solvating helium density around a molecule as a function of different rotational states.

We investigate the validity of adiabatic following here by comparing the helium density derived from quantum calculations that make full incorporation of the molecular rotation, with densities derived from calculations with a nonrotating molecule. Formally, this constitutes a comparison between a classical ground state, nonrotating molecule, with a quantum rotor in its zero energy state. It does not correspond exactly to either of the above-mentioned situations, but it does nevertheless allow a direct assessment of the influence of quantum mechanical rotational kinetic energy of the molecule on the helium distributions. We note that direct probing of both the classical and quantum criteria described earlier is problematic. Performing calculations with a classically rotating molecule surrounded by a bosonic quantum fluid is neither trivial nor an appropriate dynamical description. On the other hand, the quantum molecular rotational states are not true eigenstates of the cluster, so that evaluating the helium density for a pure molecular rotation state would also present both technical and theoretical problems. For example, the cluster ground state contains a mixture of molecular rotational states, and cannot be taken to contain solely the $j=0$ molecular state. In contrast, the comparison of a fully quantum ground state calculation for a cluster containing a nonrotating molecule with a fully quantum ground state calculation for a cluster containing a rotating molecule is well defined and has a clear interpretation. The energetic difference between these two calculations gives the hindered rotation energy increment discussed earlier. As noted in the previous sections, this energy increment can be significantly larger than the difference between low lying rotational states of the molecule.

The difference in helium distributions projected into the molecular frame provides a measure of the effect of the quantum molecular rotation on the adiabatic following by helium. A quantitative comparison between these distributions in cluster ground states containing a nonrotating and a rotating molecule will constitute the measure of adiabatic

following studied here. This comparison may differ from results of a comparison of the dependence of densities upon the total cluster angular momentum J. We will discuss this in the following explicitly for $N=1$ complexes of the linear molecules for which we have exact solutions for different J values from the collocation calculations (Sec. IV D).

B. Quantification of the effects of rotation

We now use the previously defined F and U (favorable and unfavorable, respectively) axes to define a quantifier of adiabatic following in an anisotropic molecule–helium system. An appropriate way to evaluate the effect of rotations for a cluster containing a molecule that interacts with helium via an anisotropic potential, is to define the following quantity:

$$Q(r) \equiv \frac{[\rho_U/\rho_F]_{\text{no rot}}}{[\rho_U/\rho_F]_{\text{rot}}}. \tag{1}$$

The subscripts "rot" and "no rot" are self-explanatory, referring to calculations made with inclusion or absence of the molecular rotational degrees of freedom, respectively. The term ρ_{axis} refers to the density along a particular axis defined in the molecular frame, and r is the distance from the molecular center-of-mass. As noted earlier, we use the notation "F" for an axis of the molecule that is energetically favored for helium binding and consequently has a high helium density, while "U" refers to an axis that is energetically disfavored for helium binding and consequently has a low helium density. For example, for the octahedral SF_6 molecule, F is chosen to be the C_3 axes, passing through the global minimum of the SF_6–He interaction potential, and U is chosen to be the C_2 axes, passing through saddle points of the interaction. As long as a consistent choice of privileged axes F and U is made in the rotating and nonrotating molecule calculations, the actual choice of these is subject to considerable flexibility. The main requirement is that the helium densities along these two axes be distinguishable and also measurable (i.e., nonzero). Note that these axes are not necessarily equivalent to the principal axes of the molecule, which are determined solely by the internal molecular mass distribution.

Thus, some anisotropy in the molecule–helium interaction is essential for a meaningful analysis of $Q(r)$. The obvious choice for F is a molecular frame axis that passes through the potential minimum. The choice for U is less obvious and may present several options. Clearly this should be an axis passing through unfavorable, high potential energy configurations, such as a saddle point of the molecule–helium potential energy surface. These saddle points are obtained as maxima of the potential curve obtained when a single helium atom rotates (adiabatically) around the molecule, i.e., the curve is obtained by optimizing the radial coordinate from the molecular center-of-mass to obtain the minimum energy for each rotational angle. When the maximum of the resulting potential curve obtained is very high, and if the curve presents local minima, then there exist multiple saddle points, and multiple options for the U axis are possible. We prefer to choose a saddle point which does not

provide an extreme energy difference between F and U, to avoid problems arising from density zeros in Q. For example, for the octahedral SF_6 molecule, the U axis is better chosen as the C_2 rather than the C_4 axis that is the highest energy symmetry axis. In general, we shall refer to the molecular frame axes F and U as "privileged axes" rather than as symmetry axes, since for lower symmetry species such as HCN and OCS, these axes will not reflect any particular symmetry of the interaction potential.

The ratios in the numerator and denominator of Eq. (1) compare the density in the region of the potential minimum to that in the region of a much less favorable point such as a saddle point. These axes are always defined in the molecular frame, whether this is rotating or not. If there is complete adiabatic following, the densities obtained with and without rotations would be identical and we would have $Q \equiv 1$. Conversely, if there is little or no adiabatic following, the helium density would not be significantly modulated by the molecular potential contours. This leads the denominator of Q to approach unity while the numerator would remain small. Thus, smaller values of Q are indicative of a lack of adiabatic following. It is important to note that this assessment applies only to a molecule possessing an anisotropic interaction with helium and hence having the possibility of some angular modulations in the helium density in the molecular frame. For an isotropic interaction, there can be no angular modulations of the helium density and hence the ratio of densities in both numerator and denominator of Eq. (1) is unity, regardless of the choice of axes F and U. Also, since the anisotropy generally decreases as the distance from the molecule increases (see, e.g., Figs. 1, 3, 5, and 6), $Q(r)$ $\rightarrow 1$ as $r \rightarrow \infty$. We expect that other physical factors that can make the density more isotropic can also reduce the usefulness of this estimator. In particular, for larger cluster sizes the primarily repulsive helium–helium interaction acts to distribute the helium atoms evenly over the configuration space, opposing the focusing effect of the global potential minimum of the molecule–helium interaction. If the latter is strong, the helium–helium interaction is not very important, and Q remains a sensitive discriminator for $N>1$. We will see that SF_6 falls into this category. However, if the molecule–helium interaction is weak, the helium–helium interactions may dominantly influence the behavior of the density ratios, making them appear isotropic. We will see that this is the situation with the lighter HCN molecule for $N>1$.

An analogous quantity to Eq. (1) can be defined in terms of the helium wave functions, by replacing the densities by the projections of the N-particle helium wave functions into the molecular frame. Preliminary results with this quantifier were presented in Ref. 7. We show in the following, with the example of SF_6, that these two related quantifiers of adiabatic following provide consistent results, and that either can therefore be used to analyze the phenomenon. Overall, these considerations lead us to expect that $Q(r)$ will provide a useful quantification of adiabatic following when applied to clusters within the first solvation shell for molecules possessing an anisotropic molecule–helium interaction potential. This will work for $N=1$ and possibly for larger N values,
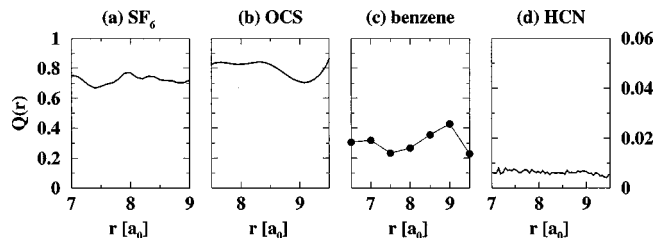

FIG. 8. Plot of the adiabatic following quantifier $Q(r)$ for the $N=1$ complexes: (a) SF_6–He, (b) OCS–He, (c) C_6H_6–He, and (d) HCN–He. $Q(r)$ is defined in Eq. (1). See the text for discussion and definition of the privileged axes for each molecule. Due to the extremely small $Q(r)$ values for HCN, the y-axis scale for (d) is considerably expanded relative to the [0-1] range used in panels (a)–(c).

depending on the relative magnitudes of the helium–helium and helium–molecule interactions.

C. Q analysis for $N=1$

Figure 8 shows the behavior of $Q(r)$ for the various $N=1$ complexes studied in this paper. In each case we have plotted $Q(r)$ over the region in which there is appreciable density along both of the privileged axes.

1. SF_6

Figure 2 shows that for SF_6 the mixed density along the C_4 axis is very low in both rotating and nonrotating molecule calculations. The use of this axis as the privileged axis U leads to small values of both numerator and denominator in Eq. (1), which would introduce a large numerical inaccuracy. We thus choose to use the C_2 axes for the U axis for SF_6. The resulting behavior of $Q(r)$ in the region of appreciable density along both privileged axes F (C_3) and U is shown in Fig. 8(a). We see that within this physically significant region Q is approximately 0.7, noticeably less than unity, indicating that for rotation of SF_6 the adiabatic following by helium is not complete, even for $N=1$.

These results for SF_6–He are not tied to a particular choice of trial wave function, or to the definition of $Q(r)$ in terms of the density in Eq. (1). This is easily demonstrated by performing unbiased DMC calculations, which yield representations of the wave function directly without any *a priori* assumptions. Of course, this kind of analysis is restricted to smaller clusters, for which sampling efficiency is not an issue.[15] With unbiased DMC we can analyze the wave function directly. As expected, the wave function profiles exhibit the same features as the density profiles in Fig. 2.[33] Evaluating the adiabatic quantifier $Q(r)$ with projected wave functions in Eq. (1) instead of densities,[7] results in a similar average value of $Q(r) \sim 0.7$, shown in Fig. 9. This confirms the conclusion of the importance-sampled calculations (Fig. 8) that there is a significant but not complete degree of adiabatic following in this system. As long as a consistent definition of densities or of wave functions is employed in Eq. (1), similar magnitudes of Q are found.

Figure 9 also shows the results of a simple test of the sensitivity of $Q(r)$ to the magnitude of the gas phase rotational constant B_0.[3] Replacing the rotational constant $B=B_0$ in the simulation with $B=10B_0$ is equivalent to reduc-
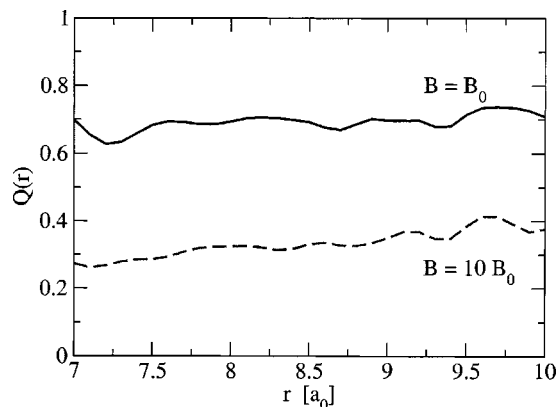
J. Chem. Phys., Vol. 118, No. 11, 15 March 2003

Doped ^{4}He clusters   5019

FIG. 9. $Q(r)$ for SF_6–He, computed using unbiased DMC and evaluated using wave function projections instead of densities in Eq. (1) (Refs. 7 and 33). The effect of changing the value of B used in the simulation from $B = B_0$ to $B = 10B_0$ is shown. [B_0 is the gas phase rotational constant value, B is the diffusion constant governing the rotational moves in IS-RBDMC (Ref. 15)].

ing the moment of inertia by a factor of 10, or, conversely, to increasing the (classical) molecular rotation rate. Figure 9 shows that the $Q(r)$ curve for the artificially faster rotor is much lower, indicating that the helium density is now *less* able to follow the rotation of the faster dopant molecule.

2. OCS

For OCS, we again use the chosen F and U axes to define $Q(r)$. The very small density along the U′ axis removes this from consideration as the unfavorable privileged axis (see the earlier discussion for SF_6). The behavior of $Q(r)$ for OCS over the range of r values for which the U axis density is appreciable (see Fig. 4) is shown in Fig. 8(b). The average value of $Q(r)$ over this region is ~ 0.8. Thus, just as for SF_6, the adiabatic following by helium is significant but is not complete for OCS, even at $N = 1$.

3. Benzene

The $N = 1$ He–benzene density is not as easily amenable to analysis in terms of Q as that of the other complexes because the strong localization of the helium density at the global potential minimum leads to very small values of the density along the U directions. We therefore take somewhat larger bin sizes when sampling along the privileged axes for this molecule in order to reduce the statistical fluctuations deriving from small values of the density. This allows us to obtain only a few values of $Q(r)$ in the region of interest, namely where the density along the U direction is non-negligible. The sampling is made over all equivalent axes, as noted earlier for SF_6. We see in Fig. 8(c) that the resulting value of Q fluctuates around an average of ~ 0.3. This value is markedly smaller than that obtained for the SF_6 molecule, which has a similar potential well depth with helium. We attribute this partly to the difference in shape of the potential minimum, with that for benzene being broader and allowing more displacement of the helium density upon rotation. It is also consistent with the fact that the hindered rotation increment is significantly larger for the benzene–He complex than

for the other complexes. The greater energetic cost to incorporating the molecular rotation for benzene within the helium complex appears to correlate with a greater difficulty of adiabatic following by the helium density. In this case the high degree of anisotropy in the interaction potential outweighs the simple expectations based on consideration of the molecular mass, resulting in a highly individual response.

4. HCN

The diffuseness of the helium distribution around this lighter molecule introduces additional technical requirements. In particular, binning the density along the z axis is not easy since this axis is located at the edge of the binning region. We prefer to use a finite volume in order to evaluate the Q factor. To implement this constraint, we count the number of walkers included in a slice $[r, r + \Delta r]$ of a cylinder of radius 1 a_0 that is centered on the z axis. The ratio of these quantities with and without the molecular rotation is a good approximation of the corresponding ratio of densities. It was confirmed that small variations in the radius of the cylinder do not affect the results for the ratio $Q(r)$.

The large variation in density between the two privileged axes translates to a negligible value of $Q(r)$, shown in Fig. 8(d). Note the different scale used in the y axis for this panel, relative to that used for the heavier molecules in panels (a)–(c). In fact, the average value of Q for HCN is approximately zero (it corresponds to ~ 0.01 of the corresponding values for SF_6 and for OCS). This nearly zero value of Q indicates that adiabatic following is practically negligible in this system.

Our conclusion concerning the degree of the adiabatic following for HCN arrived at using the Q factor is in agreement with the conclusions reached independently from the classical criterion proposed in a path integral study.[7] We note that since the CPU requirement to evaluate the adiabatic following quantifier Q by IS-RBDMC is smaller than the cost of path integral calculations, it therefore presents a very useful and practical diagnostic of adiabatic following.

We interpret the very small value of Q for HCN to mean that the assumption of adiabatic following is invalid for this system, an assertion that is supported by the fact that hydrodynamic calculations assuming adiabatic following have failed to give results that are reconcilable with experiment.[5,6,30]

D. Rotational state dependence of densities for $N=1$

As discussed in Sec. IV B, analysis of rotational state dependence of densities in a quantum calculation provides a close analog to the classical qualitative picture. For the linear $N = 1$ complexes, computation of exact energies and eigenfunctions is possible using basis set expansion methods such as the collocation method.[20] For these small systems we can then examine the helium density dependence upon the total angular momentum of the complex, J. This provides an interesting contrast with the comparisons between ground state ($J = 0$) calculations made with and without molecular rotation. We have performed collocation calculations for the $N = 1$ complexes with the linear molecules HCN and OCS (see
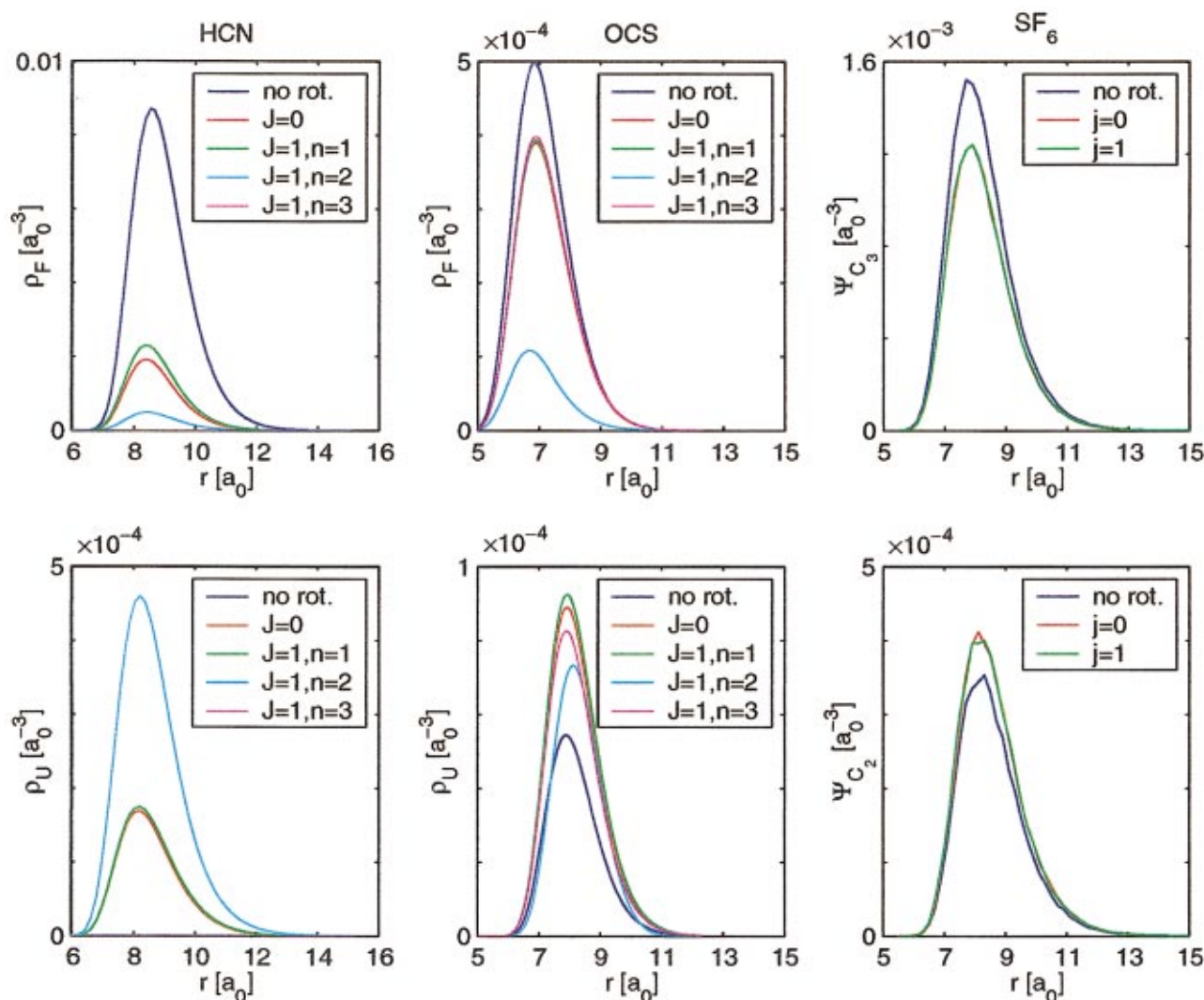
FIG. 10. (Color) Comparison of helium densities along favorable (F) (upper panels) and unfavorable (U) axes (lower panels) for HCN, OCS, and SF_6. Several calculations are represented here by the different colored lines. (i) Calculations neglecting molecular rotation (dark blue lines). (ii) Calculations incorporating molecular rotation, for the $J=0$ complex state (red lines). (iii) Calculations incorporating molecular rotation, $J=1$ complex state (green lines, "$J=1$, $n=1$;" cyan lines "$J=1$, $n=2$;" magenta lines, "$J=1$, $n=3$"). The three sublevels for $J=1$ are labeled in order of increasing energy, with $n=1$ the lowest energy level. See the text for definitions of F and U for HCN, OCS, and SF_6.

the Appendix for details) and then projected the helium component of the eigenfunctions into the molecular frame to obtain the corresponding helium densities for low-lying rotational states. Figure 10 presents these densities obtained along the F (upper set of panels) and U (lower set of panels) directions for HCN–He (left) and OCS–He (center), for the $J=0$ ground state and for the three $J=1$ rotationally excited states. Each panel also shows the result for a nonrotating molecule (obtained by setting the molecular rotational constants A,B,C equal to zero in the collocation calculations). To provide comparison with a nonlinear molecule, the right-hand panels show the analogous results for the $J=1$ state for SF_6 obtained using unbiased DMC with the fixed-node approximation.

Several systematic features are evident in Fig. 10. First, the collocation results for both HCN and OCS confirm that the introduction of the molecular rotation has a significant effect on the helium densities in the $J=0$ state—compare the blue line (nonrotating molecule) with red line (rotating mol-

ecule). Second, for both linear molecules, the density of the lowest $J=1$ state (green line) is very similar to that obtained for the ground state (red line). The densities for the corresponding lowest $J=2$ states (not shown) are also very similar to that of the ground state. However, the density in the other $J=1$ and $J=2$ sublevels can be significantly different (cyan and magenta lines). Examination of the wave functions for the states shows that this is due to the presence of nodal structure in the frame attached to the molecule, which complicates a direct comparison of the densities. For example, for HCN–He, the third $J=1$ state ($n=3$ in Fig. 10, denoted with the magenta line) has a node on the molecular axis itself. Referring to Fig. 6 reveals that this corresponds to both the F and U directions, explaining why this $J=1$ sublevel shows a zero value in both upper and lower panels of Fig. 10. In contrast, the lowest $J=1$ and $J=2$ sublevels have little or no nodal structure in the molecular frame, resulting in a similar shaped helium distribution to that of the ground state in Fig. 10. The nodal structure in the molecular frame

for these states can be easily recognized in the complete two-dimensional representation of the wave functions for OCS–He and HCN–He given in Ref. 34.

For the SF_6 complex within the fixed-node approximation (right-hand panels in Fig. 10), the difference between the $J=0$ and $J=1$ helium densities is now very small relative to the difference between the $J=0$ calculations made with and without molecular rotation. In addition, all three $J=1$ sublevels have identical density distributions in the molecular frame. Given our analysis of the behavior of the HCN and OCS complexes in the exact calculations presented earlier, this simpler behavior can now readily be understood as a consequence of the imposition of a fixed nodal structure in the molecular angular degrees of freedom in the laboratory frame. The smaller difference between the $J=0$ and $J=1$ helium densities is due to a rigorous decoupling of the nodal surface from the molecular frame in this particular fixed node approximation. This holds for all $J=1$ sublevels, and therefore there is no differentiation of the density in the molecular frame for different sublevels. We note that this fixed node approximation has been shown to provide accurate results for the rotational energies of the $N=1$ complex,[3] while the analogous fixed node approximation for the similar mass OCS molecule has been shown to provide poor accuracy for $N=1$.[9] The analysis of the density dependencies for the two molecules made here suggests that the accuracy of this fixed node for SF_6 is probably due to the high symmetry of this molecule.

Several general conclusions may be drawn from this analysis of the rotational state dependence of the helium densities in the molecular frame for the $N=1$ complexes. First, it is apparent from the examples of molecules with different mass and different symmetry shown here, that the effect of adding molecular rotational degrees of freedom to calculations of the ground state density is greater than that of increasing the angular momentum of the complex from $J=0$ to 1. This is true not only for the heavier molecules OCS and SF_6 for which the hindered rotation energy increment is larger than the energy difference between these two levels, but also for the lighter HCN molecule, for which the hindered rotation energy increment is slightly less than the energy difference between $J=0$ and $J=1$ (1.55 compared to 2.40 cm^{-1}, respectively). Thus we can conclude that this is a very general effect. Second, we see that comparison of the rotational state dependence is only really simple when there is no rotational nodal structure in the molecular frame, i.e., when this is located primarily in the molecular orientational degrees of freedom in the laboratory frame. Consequently a simple systematic analysis of the helium density in the molecular frame for all rotational states is not feasible. The $J=1$ sublevels analyzed here showed nontrivial variations of the density when the levels contained nodal structure in the molecular frame. A corollary of this is then a cautionary note that an analysis of the densities obtained for excited states based on a classical picture of molecular rotation (Sec. IV A) is not meaningful since a classical analysis does not include the notion of nodal structure. Finally, while we have seen little difference of the helium density between $J=0$ and $J=1$ (within the caveats about the effect of nodal structure in the molecular frame), this situation may change for much higher rotational states, J.

V. RESULTS FOR $N>1$

For larger numbers of helium atoms, the full cluster potential was obtained by adding the HFD-B potential of Aziz and co-workers for the He–He interactions[24] to the molecule–helium interactions that were employed for the $N=1$ complexes in Sec. III. When $N>1$, as noted in Sec. IV B, the effects of the He–He interaction on the density and Q factor must be carefully considered. Generally, the helium–helium repulsion will favor an evenly distributed, i.e., more isotropic, helium density. Far away from the dopant molecule, the dopant–helium interaction (V_{X-He}) is also weak and becomes increasingly isotropic. Thus, at large distances r, one would not expect much variation in the helium density between calculations with and without rotations included. For this reason, when computing Q for $N>1$, we must focus our attention close to the dopant molecule. In particular, we examine the region near the peak of the first solvation shell. In this section we show how Q is modified by the additional He–He interactions in larger clusters, considering first the heavier molecules SF_6 and OCS, then the more anisotropic C_6H_6 molecule, followed by the considerably lighter HCN molecule.

Table II shows how the ground state energy of larger $SF_6–He_N$ clusters depends on N, for calculations made with and without the molecular rotation. It is evident that for $N \leq 6$, the difference $\Delta E/N$ between the total energy per particle with and without rotation is approximately constant. This supports our identification of this difference for $N=1$ as a measure of the zero point energy of the hindered SF_6 rotation in the effective potential field provided by the surrounding helium density. (For larger cluster sizes this difference becomes an increasingly smaller percentage of the total energy and even greater sampling than made here (Table VIII)

TABLE II. $SF_6–He_N$: IS-RBDMC total energies and energies per host particle in cm^{-1}. The ''no rot'' columns contain the energies obtained when SF_6 rotations are turned off in the calculation. $\Delta E \equiv E - E_{no\,rot}$.

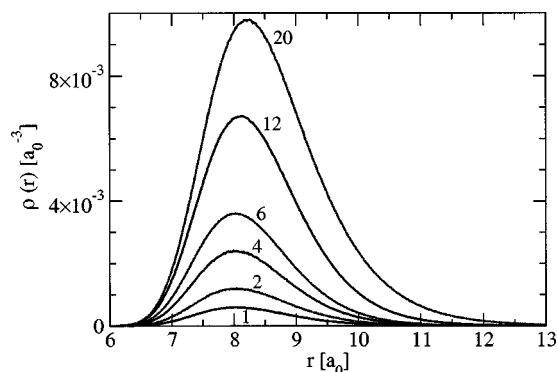| N	E	$E_{no\,rot}$	ΔE	E/N	$E_{no\,rot}/N$	$\Delta E/N$
1	$-25.8(2)$	$-26.6(2)$	0.8(4)	$-25.8(2)$	$-26.6(2)$	0.8(4)
2	$-52.2(3)$	$-53.9(2)$	1.7(5)	$-26.1(1)$	$-26.9(1)$	0.9(3)
4	$-105.8(5)$	$-109.7(4)$	3.9(9)	$-26.4(2)$	$-27.4(1)$	1.0(2)
6	$-159.6(7)$	$-165.2(7)$	5.6(13)	$-26.6(1)$	$-27.5(1)$	0.9(2)
12	$-299(3)$	$-304(2)$	5(5)	$-24.9(2)$	$-25.4(2)$	0.5(4)
20	$-427(8)$	$-433(7)$	6(14)	$-21.3(4)$	$-21.6(3)$	0.3(7)

FIG. 11. Integrated radial density profiles for SF_6-He_N, $N = 1,2,4,6,12,20$. All profiles exhibit a single peak that grows with N, showing that the first solvation shell is still being filled for $N \leqslant 20$. Reference 40 contains profiles for larger clusters sizes having additional shells populated.

FIG. 13. Plot of the adiabatic quantifier $Q(r)$ for clusters having $N>1$ helium atoms, for SF_6, OCS, benzene, and HCN. The legend for panel (a) is valid also for panels (b) and (d). (a) SF_6-He_N: $Q(r)$ for $N=4,6,12,20$. $Q(r)$ is plotted only in regions of appreciable density along the U (C_2) axis (see Fig. 11). (b) $OCS-He_N$: $Q(r)$ for $N=4,6,12,20$. $Q(r)$ is plotted only in regions of appreciable density along the U axis (see Fig. 4 and Ref. 35). The curves were obtained by taking ratios of fitted (and smoothed) mixed density profiles. (c) $C_6H_6-He_N$: $Q(r)$ for $N=3,14$. $Q(r)$ is plotted only in regions of appreciable density along the U axis (see Figs. 5 and 14). (d) $HCN-He_N$: $Q(r)$ for $N=4,6,12,20$. Note that the values for $N>12$ approach unity, indicative of a more isotropic effective potential for the outer atoms (see the text).

would be required to evaluate this difference with the required error bars.) The integrated radial helium density profiles for SF_6-He_N are shown in Fig. 11. These are mixed densities, shown for cluster sizes $N=1,2,4,6,8,12,20$. It is evident from Fig. 11 that we are still within the first solvation shell for all these sizes. The corresponding radial density profiles for OCS are provided in Ref. 35, together with two-dimensional mesh plots of the full densities and the corresponding energetics. We show the full angular variation in the density around SF_6 for $N=4$ in Fig. 12, comparing as usual the data for calculations made with and without the molecular rotation. Figure 12 was produced by first symmetrizing the raw data (summing the contributions from all equivalent bins) and then interpolating the Cartesian data onto a spherical shell. This kind of visual comparison between angular variations for SF_6, made originally for projected wave functions in Refs. 3 and 7, provided the initial impetus for our current quantitative analysis of adiabatic following. The smearing out of the helium density when SF_6 rotation is incorporated is highlighted in panel (c), which shows the difference density between panels (a) (no molecular rotation) and (b) (including molecular rotation). [The color scale in (c)] is different from that in (a) and (b), and
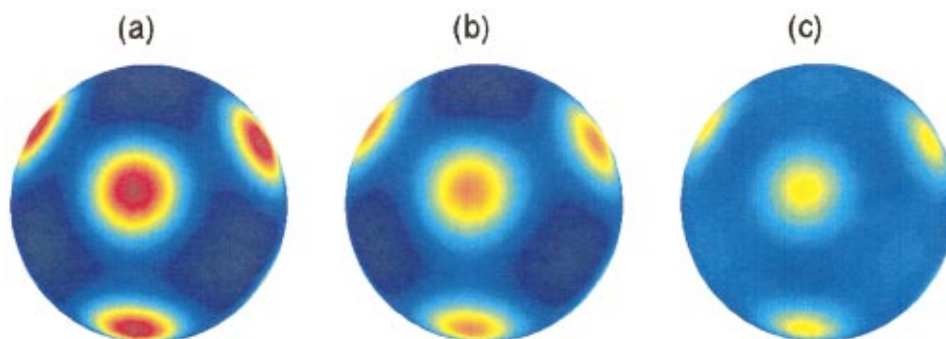
was adjusted to provide maximum contrast between high and low regions.) A complete set of analogous plots for all available cluster sizes up to $N=20$ is given in Ref. 34.

The Q values extracted from these densities for SF_6- and OCS-doped clusters with up to $N=20$ helium atoms are shown in Figs. 13(a) and 13(b). We see that for these relatively strongly bound molecules, Q continues to provide a sensitive measure of the degree of adiabatic following for $N>1$, remaining fairly stable as a function of r for the smaller sizes, and showing a small but noticeable increase with r for the larger sizes. For SF_6, for which the highest quality data are available, with the largest amount of sampling (see Table VIII), there is evidence of some size dependence. Comparing also with Fig. 8 we see that there is a small decrease in Q on going from $N=1$ to $N=6$, and that subsequently Q increases again, approaching unity as N increases above 12. The increase in average Q at larger N can be attributed to the effect of helium–helium interactions in driving toward a uniform helium distribution, as discussed earlier. This effect is seen to a much greater extent in the case of HCN in the following. The decrease in Q seen for the

FIG. 12. (Color) Angular variation of $\rho(\mathbf{r})$, the ground state helium density, measured at $r=8\,a_0$ from the SF_6 molecule, and displayed as a color coded cut on a spherical polar grid located on a ball of radius r. The densities are mixed densities obtained from IS-RBDMC (see the text). (a) No molecular rotation, i.e., for a nonrotating SF_6. (b) Including molecular rotation of SF_6. (c) Difference density, defined as (a) and (b), emphasizing the greater localization of the densities in (a). The molecule-fixed S–F axes are oriented along the x, y, and z axes. The chosen distance $r=8\,a_0$ is located on the inner edge of the radial profile of the first solvation shell peak (see Fig. 11). The density peaks are located in the C_3 angular orientations. The color scale goes from blue (lowest density) to red (highest density). Panels (a) and (b) have the same dynamic range for the color scale. The dynamic range of the color scale in panel (c) was expanded to better visualize the difference.
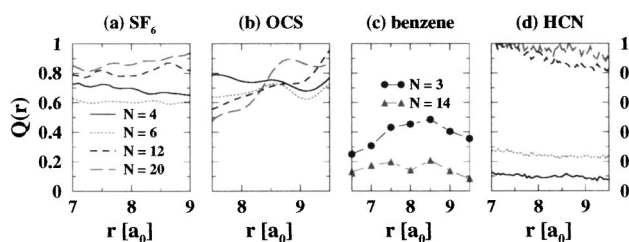
smaller sizes is less straightforward. We attribute this to a delicate balance between the localizing effect of the anisotropic SF_6–He anisotropic interaction close to the molecule, and the repulsive He–He interaction. As the cluster size increases, the He–He contributions become relatively more important, eventually dominating the total energy and also the structure. This trend with N is consistent with the behavior of Q as a function of r. While the data for OCS in Fig. 13(b) are noisier and do not allow such firm conclusions about size dependence to be made, it does appear to show similar trends in $Q(r)$ with both r and N. Overall, this detailed discussion for $N>1$ shows that there are multiple factors determining the actual value of Q for any given cluster size N and distance r. We emphasize that the most significant observation is that $Q(r)$ remains sensitive to the potential anisotropy at small r values, even for the largest cluster sizes.

The Q values for larger benzene clusters are shown in Fig. 13(c), for $N=3$ and $N=14$. As mentioned previously, analysis of the $N=1$ benzene–He complex in terms of Q was harder than for the SF_6 and OCS molecules, because for benzene most of the single helium atom density is localized along the F direction and the density along the U directions is very small. As more helium atoms are added to benzene, however, the secondary potential minima become occupied, and the density along the U directions increases. This is ac-
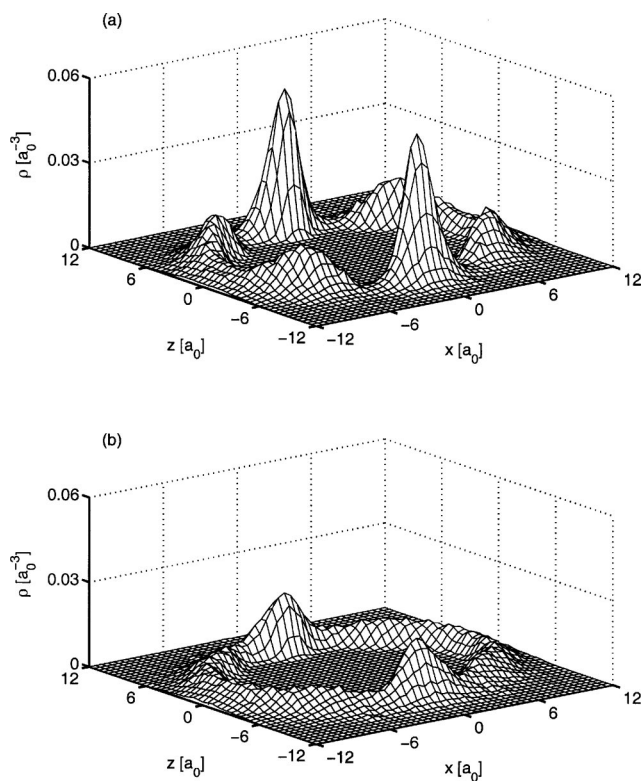

companied by an increase in the delocalization of helium atoms residing at both the global and secondary potential minima. This is illustrated in Fig. 14, which also shows the overall very dramatic difference between the densities evaluated without and with the molecular rotation. The increased density along the U directions for larger N now allows for a more stable evaluation of Q, shown in Fig. 13(c). We see that for $N=3$ the average value of Q is similar to that for $N=1$, while for $N=14$, Q decreases to an average of ~ 0.1. Bearing in mind that for benzene $N=14$ constitutes considerably less than a full solvation shell,[14,36] we conclude that this decrease is similar to that seen in panels (a) and (b) for SF_6 and OCS, and is due to competition between the molecule–helium and helium–helium interactions. Clearly the very strong anisotropy of the benzene–helium interaction causes a unique size dependence of Q that differs in detail from the other two heavy molecules. We expect that, similar to SF_6 and OCS noted earlier, Q will increase again at larger sizes and show a similar trend to saturation at large r as N approaches a full solvation shell ($N \geqslant 30$[14,36]).

In general, the small finite values of Q seen here for benzene are best understood as yet another example of the lack of complete adiabatic following of the helium density close to the molecule within the first solvation shell. The surprising aspect of these results for benzene is their low value relative to that found for SF_6 and OCS. This implies that, despite the strong spatial localization of helium at the aromatic ring, there is nevertheless only weak adiabatic following. As noted earlier for $N=1$, this unique response of the benzene molecule indicates that not only the strength of the molecule–helium interaction, but also the shape of the potential minimum and the general topology of the potential surface is important in determining the propensity of the helium density to distort with molecular rotation.

TABLE III. Minimum, maximum, and average Q values for SF_6–He_N, computed over the range $7.5a_0 < r < 8.5a_0$ with unbiased DMC, and evaluated by substituting the density projections with wave function projections in Eq. (1).

N	Q_{min}	Q_{max}	Q_{avg}
1	0.68	0.71	0.69
3	0.68	0.70	0.69
4	0.66	0.70	0.68
5	0.63	0.65	0.64
6	0.65	0.67	0.66
8	0.68	0.74	0.71

FIG. 14. Helium density around a benzene molecule in benzene–He_{14}, shown as cuts through the $y=0$ plane, calculated by IS-RBDMC. (a) Calculations without molecular rotation. (b) Calculations incorporating molecular rotation. The densities are evaluated here by descendant weighting and are symmetrized to reduce statistical fluctuations. The $y=0$ plane bisects two carbon–carbon bonds (see Fig. 5), and consequently contains four secondary helium density peaks in addition to the two primary helium density peaks located near the global minimum (see the text).

TABLE IV. Hindered rotation energy increment for $N=1$ complexes, $\Delta E_0 = E_0(R) - E_0(NR)$, where R and NR refer to calculations with and without the molecular rotation, compared with gas phase rotation constant B_0 and molecular mass m for the four molecules studied here. E_0 is the ground state energy. Units of E_0 and B_0 are cm^{-1}, and m is in u.

Molecule	ΔE_0	B_0	m
SF_6	0.7	0.091	146
OCS	1.2	0.07	60
HCN	1.55	1.2	27
Benzene	2.97	0.188, 0.0938	78

The case of the lighter HCN molecule is very different from these heavier molecules, as was already evident with the $N=1$ cluster (Fig. 8). Since no appreciable adiabatic following was found for $N=1$ [Fig. 8(d)], one physically expected conclusion is that this will also be the case for $N>1$. Figure 13(d) presents the behavior of $Q(r)$ obtained for HCN–He_N with N up to 20. We see however, that while approximately constant with r, the value of the function $Q(r)$ monotonically increases as a function of N, reaching its maximal value of 1 for $N\simeq12$. The reason for this monotonic increase in $Q(r)$ as N increases is a stronger version of the effects seen with SF_6 in Fig. 13(a) for $N\geq6$ and discussed earlier. It reflects the increasingly dominant role of the He–He interaction in determining the helium distribution in the first solvation shell for the calculation with nonrotating HCN. The attraction of helium atoms by linear HCN is both weaker and more isotropic than the corresponding attraction by the heavier linear species, OCS (compare Figs. 6 and 3). Consequently, helium atoms added beyond $N=1$ will eventually fill the locations defined earlier as unfavorable for the HCN–He interaction (Sec. III D), driven by the need to minimize the helium–helium repulsions. This happens whether molecular rotation is included or not, because the weak HCN–helium interaction does not provide sufficient energetic differentiation between favorable and unfavorable locations. In other words, the energy difference between the F and U axes is too small to override the tendency to a uniform angular distribution induced by the repulsive helium–helium interaction. The result is that the Q factor for HCN is very strongly N-dependent over all ranges of N, and that there is no apparent regime of competition between angular localization around HCN–He and the He–He repulsive effects. Consequently Q simply increases with N at a faster rate than for the other molecules and its behavior for HCN most clearly shows the loss of significance in $Q(r)$ as N increases to a full solvation shell and the helium–helium interactions dominate the angular distribution.

We can draw several conclusions from these systematic trends. First, for the heavier molecules, SF_6, OCS, and benzene, it is evident that the assumption of partial adiabatic following within the first solvation shell of helium remains valid for all sizes up to completion of the first solvation shell. As an independent check on this conclusion, several sizes of SF_6-doped clusters were also studied using unbiased DMC ($N\leq8$, since artificial dissociation becomes an issue with $N\geq12$[15]). The resulting Q values, evaluated from wave function projections, are summarized in Table III. We see that Q remains stable for this range of smaller sizes when evaluated by wave function projections, and that the value is quite similar to the values derived from densities [Fig. 13(a)]. Thus, it appears that, however we choose to quantify it, adiabatic following does also occur in the first solvation shell for these heavier molecules with $N>1$ helium atoms, but is similarly incomplete. Second, for these heavier molecules, the detailed behavior of Q at small N values is strongly dependent on the energetic balance between the anisotropic molecule–helium and isotropic helium–helium interaction potentials. Third, the lighter HCN molecule shows quite different behavior, with the clear quantification of negligible

adiabatic following for $N=1$ being followed by a monotonic increase in Q with N, as a result of the dominant energetic role played by the He–He repulsions in determining the angular distribution in this case. Lastly, for all molecules, as the cluster size increases to a full solvation shell, at r values lying beyond the peak of the first solvation shell, $Q(r)$ tends to unity, reflecting the increasingly isotropic density at large distances from the molecule.

VI. SUMMARY AND CONCLUSIONS

The effects of including molecular rotations in calculations of helium solvation density have been carefully analyzed here for a variety of molecules solvated in a low temperature liquid helium environment (helium droplets). Molecular rotation has a noticeable effect on both the ground state energy and the helium density distribution in a doped cluster. The energy difference between calculations with and without molecular rotation, referred to here as a hindered rotation energy increment, was seen to provide the cluster analog of matrix zero point energy. This energy increment was found to range from $\sim10\times B_0$ for the three heavier molecules SF_6, OCS, and C_6H_6, to $\sim B_0$ for the lighter HCN molecule, as summarized in Table IV. It thus correlates in a general (not quantitative) sense with the dopant mass and overall extent of anisotropy of the molecule–helium interaction. For all four molecules, we have found a significant effect of molecular rotation on the solvating helium density, regardless of the molecular mass and symmetry. The details of the density response to the molecular rotation differ amongst the molecules, and some trends with molecular mass and symmetry are apparent. In all cases the helium density in the molecular frame is considerably more delocalized in the angular degrees of freedom when it is calculated with incorporation of the molecular rotation than when it is calculated with a nonrotating molecule. This general effect is important since, as discussed extensively elsewhere,[37,38] solvating helium densities calculated for a nonrotating molecule do not correspond to eigenstates of angular momentum and this can cause problems for analysis of the dynamic helium response to molecular rotation. In particular, the greater delocalization and angular smoothness of the helium solvation density significantly lowers estimates of hydrodynamic response to molecular rotation, rendering this insignificant for a true density evaluated with angular momentum consistency.[38]

The analysis in this paper has also enabled us to provide a meaningful definition for the notion of adiabatic following of molecular rotational motions by the solvating helium density that allows a quantitative analysis. The subtleties in this notion of adiabatic following and its extent, i.e., whether partial or complete, were discussed with attention to the quantum or classical nature of the molecular rotation, to the molecular rotational state, and to the balance between the molecule–helium and helium–helium interactions. We defined an estimator $Q(r)$ that may be used to quantify the extent of this adiabatic following in the quantum situation, and that allows the variation in adiabatic following to be analyzed as a function of distance from the molecule. This estimator is applicable to molecules of general symmetry,

defining the extent of adiabatic following in terms of density ratios along privileged axes that are defined in terms of minima and of saddle points of the molecule–helium potential energy surface. It is therefore a short-range quantifier of the effect of the potential anisotropy on the helium distribution in the molecular frame, for a given molecular rotation constant and state. The estimator provides most useful information for the $N=1$ complexes, where there are no helium–helium interactions and it can act as a predictor of the extent of adiabatic following. For larger clusters the uniformizing effect of helium–helium interactions renders analysis of Q more complex. While the estimator is less useful as a predictor for $N>1$, its behavior in large clusters can be rationalized in terms of the competition between the molecule–helium and helium–helium interactions.

We have used this quantitative estimator to make a comparative study of the extent of adiabatic following by helium in four different molecule-doped helium cluster systems. We find that in none of these four cases is the adiabatic following by helium complete, regardless of the mass and symmetry of the molecule, and of the number of helium atoms attached to this. For a single helium atom, the heavier molecules, SF_6 and OCS, show $Q \sim 0.7-0.8$, while the benzene molecule, which shows a considerably more complex anisotropy in its interaction with helium, shows a lower value of $Q \sim 0.3$, indicating that its solvation density is nevertheless more susceptible to distortion upon addition of molecular rotation. In contrast, the lighter HCN molecule shows essentially no adiabatic following, and $Q \sim 0$. For the heavier molecules, with larger numbers of helium atoms the value of Q may initially decrease, reflecting a balance between localization due to the molecule–helium anisotropy and the helium–helium interactions that is very molecule-specific. However, as N further increases, particularly as it approaches a complete solvation shell, Q subsequently increases as the helium–helium interactions become dominant. At the largest sizes, a clear r dependence is seen to emerge, with $Q<1$ at small r inside the first solvation shell and increasing to approach unity at larger distances beyond the peak of the first shell. For the lightest molecule (HCN) Q is very sensitive to N at all sizes. For this molecule Q shows a monotonic increase with N, approaching its saturation value of unity at $N \sim 12$. This behavior for the light molecule is due to the extreme weakness of the HCN–He interaction, which is consequently quickly dominated by the packing forces deriving from the helium–helium interactions as N increases, leading to a quasi-isotropic distribution in the angular degree of freedom.

Several other factors that can lead to a unit value of Q were identified in addition to the increasing dominance of the He–He interactions at large cluster size. These include an isotropic molecule–helium interaction potential and evaluation of Q at large distances from the molecule. Evaluation of Q in higher molecular rotational states also exhibits more complex behavior and is less amenable to interpretation solely in terms of adiabatic following. Overall, we conclude that in order to ascertain the extent to which the helium density adiabatically follows molecular rotation, it is sufficient to evaluate $Q(r)$ for the $N=1$ complex, and to compare,

e.g., with the various molecules studied here. This gives a systematically varying estimator that reflects the effect of the molecule–helium interaction and both molecule and helium masses on the response of the helium density in the first solvation shell to molecular rotation. As detailed earlier, the modifications of Q for larger numbers of helium atoms can be rationalized in terms of the additional helium–helium interaction, but the values are very molecule-specific because of the competition between this and the molecule–helium interaction. Consequently different N-dependence is seen for different species, and the values of $Q(r)$ for $N>1$ are not useful for comparative evaluations of adiabatic following.

These results have significant implications for dynamical models of molecular rotational motion in helium droplets. They show that the solvating helium density can only partially follow the molecular rotation, even for the heavier molecules, and that this partial adiabatic following is confined to the immediate vicinity of the molecule within the first solvation shell. This is consistent with the conclusions of the microscopic two-fluid model,[4,7] which found that only the local nonsuperfluid density in the first solvation shell can adiabatically follow the molecular motion, while the complementary local superfluid density does not adiabatically follow. However it is in disagreement with models that assume 100% of the helium density adiabatically follows the molecular rotation.[5] The results presented here from these microscopic quantum calculations show that this assumption is incorrect and that only a fraction of the helium density is able to adiabatically follow molecular rotation in superfluid helium. The consequences of this for hydrodynamic models of the dynamic helium response to molecular rotation will be described elsewhere.[38]

ACKNOWLEDGMENTS

APPENDIX: COMPUTATIONAL DETAILS

For a single rigid molecule, a form of trial wave function possessing the correct permutation symmetry is given by the product of pair correlation terms:[39]

TABLE V. Isotropic trial wave function parameters (in atomic units) for SF_6-He_N and $HCN-He_N$.

	c	a	γ	α
SF_6	42 000	0.80	0.0	0.0
HCN	22 067	0.638	3852	0.0056

5026   J. Chem. Phys., Vol. 118, No. 11, 15 March 2003

Patel *et al.*

TABLE VI. Anisotropic trial wave function parameters (in atomic units) for OCS–He$_N$.

a_0	a_1	a_2	a_3	a_4	a_5	a_6	a_7	γ	α
-4.3	0.79	6.5	0.25	0.26	-0.18	6.4	0.92	3010	0.04

$$\Psi_T(\vec{R},\vec{\Omega}) = \prod_{p=1}^{n} \Psi_{\text{He–X}}(R_p, R_X, \Omega_X)$$

$$\times \prod_{p \neq q}^{n} \Psi_{\text{He–He}}(|R_p - R_q|), \tag{A1}$$

where the helium atom coordinates are given by R_p and the impurity coordinates and orientation are specified by R_X and Ω_X, respectively.

It was shown in Ref. 15 that simple radial trial wave functions can be used to avoid artificial dissociation. However, this choice may potentially bias the resulting density to underestimate the angular modulations, and thereby lead to bias in the quantification of adiabatic following. In order to minimize the potential effect of such bias on the Q factor, we use the same trial wave function in both calculations (with and without molecular rotation). This also avoids the need to separately optimize the angular part of the correlation term for the two cases. This procedure can be justified since we do not focus on the precise values of the density but rather on the effects resulting from including or excluding the molecular rotational kinetic energy term in the Hamiltonian. This option was used for the SF$_6$- and HCN-doped clusters. For OCS, an anisotropic molecule–helium trial function was used and the densities evaluated by second-order extrapolation to minimize any differential trial function bias for calculations made with the rotating and nonrotating molecule. The large anisotropy of the benzene–helium interaction also necessitates the use of an anisotropic trial function for C$_6$H$_6$. For the benzene calculations, the exact ground state helium distribution was sampled using descendant weighting techniques.[16,29]

The radial molecule–helium trial functions used in this article are of the form

$$\Psi_{\text{He–X}}(R_p, R_X, \Omega_X) = \exp\left[-\frac{c}{r_{pX}^5} - a r_{pX} \right], \tag{A2}$$

where $r_{pX} = |R_p - R_X|$, and X is SF$_6$ or HCN. The parameters a and c are listed in Table V. The He–He contribution is also a parametrized (Table V) radial function of the same form

$$\Psi_{\text{He–He}}(r) = \exp\left\{ -\frac{\gamma}{r^5} - \alpha r \right\}. \tag{A3}$$

The anisotropic function employed for the OCS–He trial function is obtained from a fit to the ground state wave function of the He–OCS complex[26] calculated by use of the collocation method.[19] This fitted function has the form

TABLE VII. Trial function parameters (in atomic units) for benzene–He and benzene–He$_{14}$. The first row gives the helium–helium repulsive parameter for Eq. (A3). The next four rows give the parameters for Eq. (A5), and the remaining rows give the parameters for Eq. (A6).

	$N=1$	$N=14$
γ		3674.6
c_α	6000.0	8217.7
c_β	8000.0	2546.2
a_0	0.05	0.014 378
c_0	0.06	0.007 344 8
c_γ		1.931 7
a_γ		0.156 13
$c_{\gamma'}$		1.516 5
$a_{\gamma'}$		0.095 327
$c_{\gamma''}$		2.217
$a_{\gamma''}$		0.030 121

$$\Phi_T(R,\theta,\phi) = \exp\{a_0 R^{a_1} + a_2[1 + a_3 \cos(\theta - a_4)\ln R]$$
$$+ [a_5 R^2 \cos^2(\theta - a_4) - 1]\exp(a_6 - a_7 R)\} \tag{A4}$$

where the optimized parameters a_i are given in Table VI.

For benzene–He, the trial function expressed in the molecule-fixed frame has the form

$$\Psi_{\text{He–X}}(\mathbf{r}) = \exp\left[-\sum_{\alpha=1}^{6} \frac{c_\alpha}{|\mathbf{r} - \mathbf{r}_\alpha|^6} - \sum_{\beta=1}^{6} \frac{c_\beta}{|\mathbf{r} - \mathbf{r}_\beta|^5} \right.$$
$$\left. - a_0(x^2 + y^2) - c_0 z^2 \right]. \tag{A5}$$

The parameters c_α and c_β control the short-range behavior, where $\mathbf{r}_\alpha$ and $\mathbf{r}_\beta$ represent the carbon and hydrogen positions, respectively. The intermediate and long-range behavior is modeled as an anisotropic Gaussian centered at the benzene center-of-mass, with parameters a_0 and c_0. This relatively structureless trial function becomes inadequate as additional heliums are added and a strong local structure begins to develop around the benzene molecule. For benzene–He$_{14}$, additional structure is incorporated by multiplying the trial function above with an additional factor

$$\Xi(\mathbf{r}) = \exp\left[\sum_{\gamma=1}^{2} c_\gamma e^{-a_\gamma(\mathbf{r} - \mathbf{r}_\gamma)^2} \right.$$
$$\left. + \sum_{\gamma'=1}^{12} c_{\gamma'} e^{-a_{\gamma'}(\mathbf{r} - \mathbf{r}_{\gamma'})^2} \sum_{\gamma''=1}^{6} c_{\gamma''} e^{-a_{\gamma''}(\mathbf{r} - \mathbf{r}_{\gamma''})^2} \right], \tag{A6}$$

TABLE VIII. Simulation parameters used for the DMC propagations. For the SF$_6$ doped clusters, we used 5000 configurations for the $N=12$ and 20 clusters, and 15 000 configurations for the other cluster sizes.

Molecule	n_{block}	n_{time}	$d\tau$	α	n_{walker}
SF$_6$	500	100	20–30	0.001–0.005	5000–20 000
OCS	500	200	20	0.2	2000
HCN	1200	100	20	0.1	2000
Benzene	500	150	25	0.01	2000

where $\mathbf{r}_\gamma$, $\mathbf{r}_{\gamma'}$, and $\mathbf{r}_{\gamma''}$ correspond to the positions of the global, secondary, and tertiary minima of the helium–benzene interaction potential, respectively. These terms serve to localize helium atoms at the various potential minima, and provide a much better representation of the ground state for $N > 1$ than Eq. (6) alone.[29] For the helium–helium factors, we only use the repulsive part of Eq. (4), i.e., $\alpha = 0$. The helium–benzene trial function parameters are listed in Table VII.

Table VIII summarizes the Monte Carlo parameters used for the various systems. For each molecule, we give the time step $d\tau$, the length of the block n_{time}, the number of blocks n_{block}, the average number of configurations n_{walker}, and the parameter α which controls the update of the reference energy.[15]

The collocation calculations in this work made use of a version of the Cohen/Saykally collocation code[19] obtained from Drucker and Higgins.[21] In the He–OCS calculations, we use $N^R = 30$ radial functions with $R \in [2.5{:}10.5]$Å and include rotational basis functions for the linear rotor up to $j = 14$ with $k = 0$. For HCN–He, the corresponding basis set parameters are $N^R = 30$ with $R \in [3.0{:}10.0]$Å, and $j = 9$, $k = 0$. With these bases, the energy levels are converged to an accuracy better than the number of digits given in this paper.

[1] D. Blume, M. Mladenović, M. Lewerenz, and K. B. Whaley, J. Chem. Phys. **110**, 5789 (1999).

[2] V. S. Babichenko and Y. Kagan, Phys. Rev. Lett. **83**, 3458 (1999).

[3] E. Lee, D. Farrelly, and K. B. Whaley, Phys. Rev. Lett. **83**, 3812 (1999).

[4] Y. K. Kwon and K. B. Whaley, Phys. Rev. Lett. **83**, 4108 (1999).

[5] C. Callegari, A. Conjusteau, I. Reinhard, K. K. Lehmann, G. Scoles, and F. Dalfovo, Phys. Rev. Lett. **83**, 5058 (1999).

[6] C. Callegari, A. Conjusteau, I. Reinhard, K. K. Lehmann, G. Scoles, and F. Dalfovo, Phys. Rev. Lett. **84**, 1848 (2000).

[7] Y. Kwon, P. Huang, M. V. Patel, D. Blume, and K. B. Whaley, J. Chem. Phys. **113**, 6469 (2000).

[8] A. Viel and K. B. Whaley, J. Chem. Phys. **115**, 10186 (2001).

[9] F. Paesani, F. A. Gianturco, A. Viel, and K. B. Whaley, Phys. Rev. Lett. (to be published).

[10] J. P. Toennies and A. F. Vilesov, Annu. Rev. Phys. Chem. **49**, 1 (1998).

[11] C. Callegari, K. K. Lehmann, R. Schmied, and G. Scoles, J. Chem. Phys. **115**, 10090 (2001).

[12] S. Grebenev, J. P. Toennies, and A. F. Vilesov, Science **279**, 2083 (1998).

[13] K. K. Lehmann and C. Callegari, J. Chem. Phys. **117**, 1595 (2002); physics/0109009.

[14] P. Huang, A. Viel, and K. B. Whaley, in *Recent Advances in Quantum Monte Carlo Methods, Part II*, edited by W. A. Lester, Jr., S. M. Rothstein, and S. Tanaka, Recent Advances in Computational Chemistry, Vol. 2 (World Scientific, Singapore, 2002), p. 111, physics/0203012.

[15] A. Viel, M. V. Patel, P. Niyaz, and K. B. Whaley, Comput. Phys. Commun. **145**, 24 (2002), physics/0109004.

[16] K. S. Liu, M. H. Kalos, and G. V. Chester, Phys. Rev. A **10**, 303 (1974).

[17] B. L. Hammond, W. A. Lester, and P. J. Reynolds, *Monte Carlo Methods in Ab Initio Quantum Chemistry* (World Scientific, Singapore, 1994).

[18] A. C. Peet and W. Yang, J. Chem. Phys. **91**, 6598 (1989).

[19] R. C. Cohen and R. J. Saykally, J. Chem. Phys. **95**, 7891 (1990).

[20] R. C. Cohen and R. J. Saykally, J. Chem. Phys. **98**, 6007 (1993).

[21] S. Drucker and K. Higgins (private communication).

[22] M. Hartmann, R. E. Miller, A. F. Vilesov, and J. P. Toennies, Phys. Rev. Lett. **75**, 1566 (1995).

[23] R. T. Pack, E. Piper, G. A. Pfeffer, and J. P. Toennies, J. Chem. Phys. **80**, 4940 (1984).

[24] R. A. Aziz, F. R. W. McCourt, and C. C. K. Wong, Mol. Phys. **61**, 1487 (1987).

[25] S. Grebenev, B. Sartakov, J. P. Toennies, and A. F. Vilesov, Science **289**, 1532 (2000).

[26] F. A. Gianturco and F. Paesani, J. Chem. Phys. **113**, 3011 (2000).

[27] S. M. Beck, M. G. Liverman, D. L. Monts, and R. E. Smalley, J. Chem. Phys. **70**, 232 (1979).

[28] P. Hobza, O. Bludsky, H. L. Selzle, and E. W. Schlag, J. Chem. Phys. **97**, 335 (1992).

[29] P. Huang and K. B. Whaley, Phys. Rev. B (submitted).

[30] A. Conjusteau, C. Callegari, I. Reinhard, K. K. Lehmann, and G. Scoles, J. Chem. Phys. **113**, 4840 (2000).

[31] K. Nauta and R. E. Miller, Science **283**, 1895 (1999).

[32] K. M. Atkins and J. M. Hutson, J. Chem. Phys. **105**, 440 (1996).

[33] M. V. Patel, Ph.D. thesis, University of California, Berkeley, 2001.

[34] See EPAPS Document No. E-JCPSA6-118-002311 for plots of the helium component of the wave functions for the HCN–He and He–OCS complexes in the $J = 1$ states and three-dimensional representations of the ground state helium density around SF_6 for various cluster sizes N. A direct link to this document may be found in the online article's HTML reference section. The document may also be reached via the EPAPS homepage (http://www.aip.org/pubservs/epaps.html) or from ftp.aip.org in the directory/epaps/. See the EPAPS homepage for more information.

[35] F. Paesani, F. A. Gianturco, and K. B. Whaley, J. Chem. Phys. **115**, 10225 (2001).

[36] Y. Kwon and K. B. Whaley, J. Chem. Phys. **114**, 3163 (2001).

[37] P. Huang and K. B. Whaley, J. Chem. Phys. (to be published).

[38] T. Sachse, P. Huang, and K. B. Whaley (unpublished).

[39] K. B. Whaley, *Advances in Molecular Vibrations and Collision Dynamics*, edited by J. Bowman and Z. Bačić (Academic, JAI, New York, 1998), Vol. III.

[40] R. N. Barnett and K. B. Whaley, J. Chem. Phys. **99**, 9730 (1993).